ACS OMEGA

http://pubs.acs.org/journal/acsodf

Article

Preparation and Electrochemical Properties of Cathode Materials $Ln_{2-x}Y_xCuO_{4+\delta}$ for Solid Oxide Fuel Cell

Yang Ni, Songbo Li,* Shengli An, Xu Du, and Liangmei Xue

Cite This: *ACS Omega* 2023, 8, 5545−5552

Read Online

ACCESS | Metrics & More | Article Recommendations

ABSTRACT: $Ln_{2-x}Y_xCuO_{4+\delta}$ (Ln = Pr, Nd, Sm; x = 0, 0.025, 0.05, 0.1) cathode materials were synthesized using a sol−gel method and calcination at 1000 °C for 24 h. The phase structure, coefficient of thermal expansion (CTE), electrical conductivity, and electrochemical impedance of cathode materials were characterized. X-ray diffraction (XRD) patterns show that the cell volume of each cathode material decreases with the increase in the Y^{3+} doping amount and has good chemical compatibility with the $Sm_{0.2}Ce_{0.8}O_{1.9}$ electrolyte. The thermal expansion test shows that the increase in Y^{3+} doping reduces the average CTE of $Ln_2CuO_{4+\delta}$. The conductivity test shows that Y^{3+} doping increases the conductivity of $Ln_2CuO_{4+\delta}$, and $Pr_{1.975}Y_{0.025}CuO_{4+\delta}$ has the highest conductivity of 256 S·cm^{-1} at 800 °C. The AC impedance test shows that Y^{3+} doping reduces the polarization impedance of $Ln_2CuO_{4+\delta}$, and $Pr_{1.9}Y_{0.1}CuO_{4+\delta}$ has a minimum area-specific resistance (ASR) of 0.204 Ω·cm^2 at 800 °C. In conclusion, $Pr_{1.975}Y_{0.025}CuO_{4+\delta}$ has the best performance and is more suitable as a cathode material for a solid oxide fuel cell (SOFC).

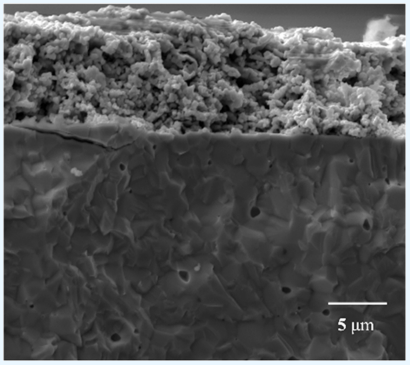

1. INTRODUCTION

The use of energy promotes the rapid development of industry and the rapid progress of human civilization. As the main force of energy supply, fossil energy needs to be converted into electric energy through heat release. This heat, which is limited by the Carnot cycle, greatly reduces the energy conversion efficiency, with a value of only 30%.[1] SOFC is one of the most promising green energy sources in the future. The commercial viability of this energy source is largely dependent on the availability of electrodes and electrolyte materials with superior properties.[2] At present, the most commonly used cathode materials are $Ln_xSr_{1-x}Co_yFe_{1-y}O_{3+\delta}$ (Ln = La, Nd), $LnBaCo_yFe_{2-y}O_{5+\delta}$ (Ln = La, Nd), etc.,[3,4] but these traditional cathode materials suffer from poor chemical compatibility, high CTE, decrease in electrical conductivity with the decrease in temperature, and other shortcomings. These problems seriously affect the application of cathode, thereby increasing the difficulty of SOFC research.[5] In the field of SOFC cathode materials, $A_2BO_{4+\delta}$ cathode materials have higher thermal stability, lower CTE, higher oxygen diffusivity, and higher surface exchange coefficient than $ABO_{3+\delta}$ cathode materials, which predict their broad prospects as SOFC cathodes.[6] Currently, studies conducted on $A_2BO_{4+\delta}$ as a SOFC cathode have shown that the doping of the A site is beneficial to improve the conductivity, oxygen diffusion, and surface exchange capacity of the cathode.[7] The replacement of A in the $A_2BO_{4+\delta}$ structure by other elements with smaller ionic radii will lead to changes in cell parameters and an increase in oxygen hyperstoichiometry.[8] Yang et al. replaced the La position with Pr with a smaller ionic radius in $La_2NiO_{4+\delta}$ and improved the electrocatalytic activity of the cathode.[9] In the $A_2BO_{4+\delta}$ structure, the $Ln_2NiO_{4+\delta}$ and $Ln_2CuO_{4+\delta}$ systems show significant mixed ion conductivity and considerable electrocatalytic activity compared with other systems. Compared with the B site of Ni, there are few studies on Cu, and Cu has been reported as a suitable doping element to optimize the property of the perovskite cathodes of SOFC. For instance, the thermal compatibility with electrolytes and electrochemical performance are improved by Cu doping in $La_{0.5}Sr_{0.5}CoO_{3-\delta}$.[10] Also, low-average TEC (13.1 × 10^{-6} K^{-1}, 50−800 °C) and Rp (0.13 Ω·cm^2@700 °C) are obtained for the Cu-doped $Bi_{0.5}Sr_{0.5}Fe_{0.8}Cu_{0.2}O_{3-\delta}$ material.[11] This study attempts to improve the electrochemical performance of $Ln_2CuO_{4+\delta}$ (Ln = Pr, Nd, Sm) cathode materials by Y^{3+} doping in the A site to change the average radius of A-site ions.

2. EXPERIMENTAL SECTION

2.1. Preparation of Cathode Materials. $Pr(NO_3)_3{\cdot}6H_2O$, $Cu(NO_3)_2{\cdot}3H_2O$, and $Y(NO_3)_2{\cdot}6H_2O$ were dissolved and then added to ethylenediaminetetraacetic acid (EDTA) dissolved by ammonia, with the molar ratio of metal cation/EDTA of 1:1.

Received: October 22, 2022
Accepted: January 17, 2023
Published: January 31, 2023

https://doi.org/10.1021/acsomega.2c06808
ACS Omega 2023, 8, 5545−5552

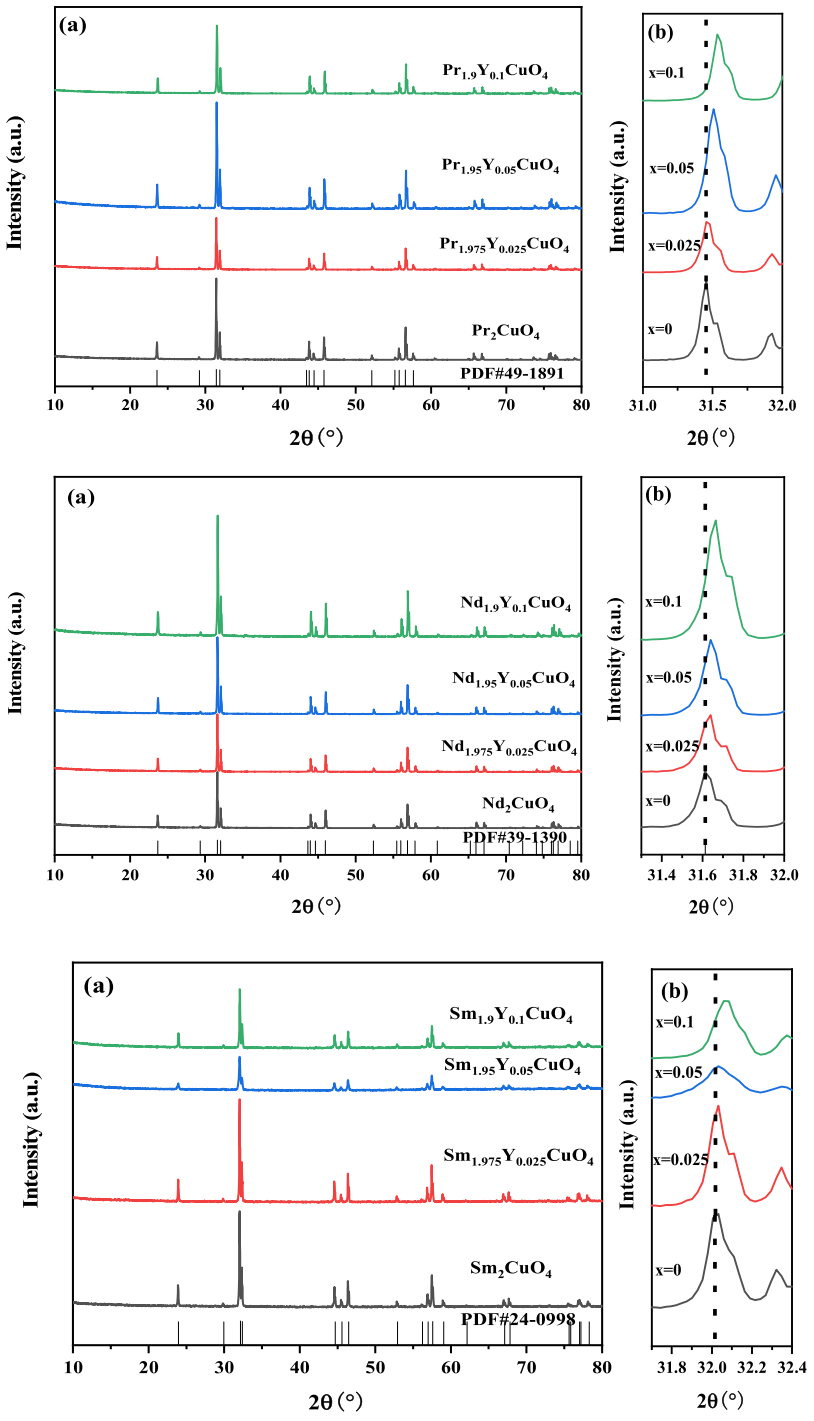

Figure 1. XRD patterns of LY_xC (x = 0−0.1) series cathode materials (a) and a locally enlarged diagram (b).

The solution was stirred for 40 min. Citric acid (molar ratio of metal cation/citric acid = 1:1.5) was added, and then the solution was stirred for 2 h. The pH of the solution was adjusted to about 7 to form the sol. A gel was formed by evaporating the water from the solution in a water bath at 80 °C. The gel was then dried and turned into a black powder precursor. The $Pr_{2-x}Y_xCuO_{4+\delta}$ cathode material was prepared by calcination in a muffle furnace at 1000 °C for 24 h after grinding the black precursor for 30 min. The $Ln_{2-x}Y_xCuO_{4+\delta}$ (Ln = Pr, Nd, Sm; x = 0, 0.025, 0.05, 0.1) sample is abbreviated as LY_xC (x = 0−0.1).

2.2. Preparation of Symmetric Cells. $Ln_2CuO_{4+\delta}$ (Ln = Pr, Nd, Sm) and $Sm_{0.2}Ce_{0.8}O_{1.9}$ (SDC) have good chemical compatibility.[12] SDC was selected as an electrolyte and prepared by calcination at 800 °C for 2 h using a sol−gel method. The electrolyte was weighed and pressed into circular sheets at a pressure of 5 MPa. The electrolyte tablets were calcined at 1450 °C for 5 h and then cooled to room temperature.

Tarpine alcohol and ethyl cellulose (with a mass ratio of 94:6) were accurately weighed, mixed, heated, and stirred to be dissolved completely and form a mixed slurry. The mass ratio of the cathode material and the mixed slurry is 4:6. The cathode slurry was obtained by grinding until the two were fully mixed. A small amount of cathode slurry was coated (screen printing method) on two sides of the electrolyte wafer. The calcination

https://doi.org/10.1021/acsomega.2c06808
ACS Omega 2023, 8, 5545−5552

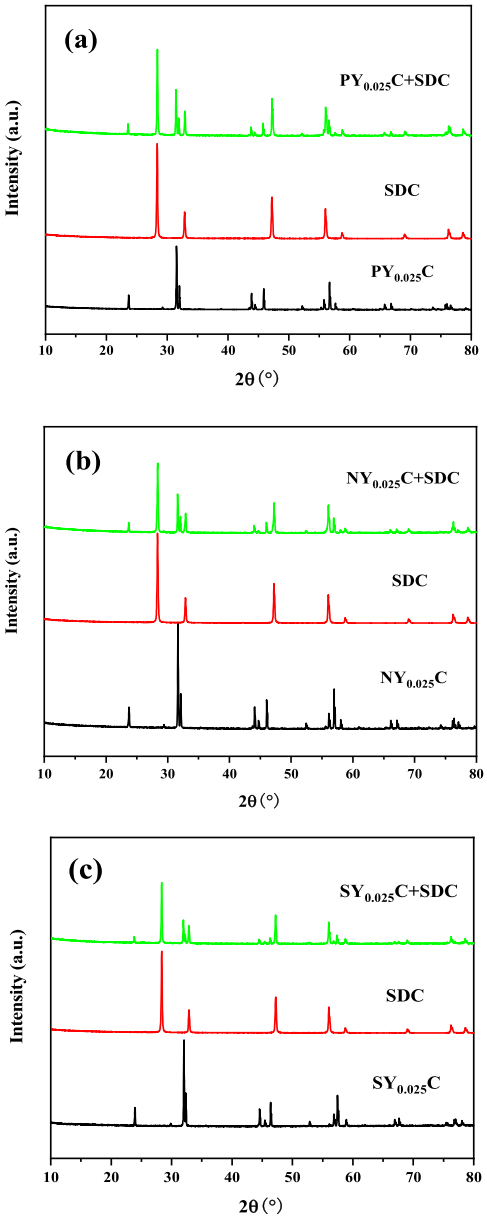

Figure 2. XRD patterns of LY_xC ($x = 0.025$) cathode material and SDC calcined at 1000 °C for 24 h: (a) $PY_{0.025}C$ + SDC; (b) $NY_{0.025}C$ + SDC; and (c) $SY_{0.025}C$ + SDC.

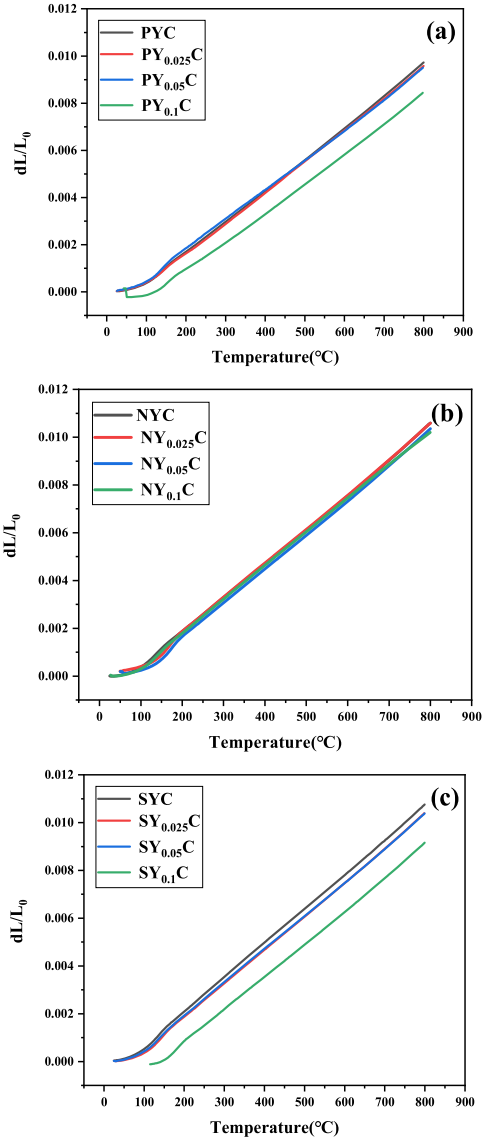

Figure 3. Thermal expansion curves of LY_xC ($x = 0$–0.1) series cathode materials: (a) PY_xC ($x = 0$–0.1); (b) NY_xC ($x = 0$–0.1); and (c) SY_xC ($x = 0$–0.1).

temperature and the time are the same as those of the cathode material. The symmetric cell was obtained after cooling.

2.3. Characterization. The structure of the cathode materials was determined by an X-ray diffractometer (Malvern Panalytical, Netherlands). A thermal expansion instrument (DIL402C, German) was used to test the thermal expansion properties. An electrochemical workstation (PGSTAT302N, Swiss) was used to test the conductivity and electrochemical impedance. The conductivity of LY_xC ($x = 0$–0.1) was determined using a dense bar specimen (20 mm × 5 mm × 5 mm) prepared by die pressing the synthesized LY_xC powder, followed by sintering at 1000 °C for 24 h in air. A standard DC four-probe method was employed for the conductivity measurement using an electrochemical workstation. Silver wires were used as the connecting leads and attached to the bar specimen surface using a silver paste followed by drying at 250 °C in the air for 2 h. The formula for calculating the conductivity σ ($S \cdot cm^{-1}$) is shown in eq 1

$$\sigma = \frac{1}{R} \times \frac{L}{A} \tag{1}$$

where A is the cross-sectional area (cm^2) of the strip sample, L is the distance from the voltage end (cm), and R is the sample's resistance (Ω).

The average CTE is calculated in accordance with eq 2

$$a = \frac{L_T - L_0}{T - T_0} \times \frac{1}{L_0} \tag{2}$$

where A is the average CTE (k^{-1}), T_0 is the initial test temperature (°C), T is the temperature of the test endpoint (°C), L_0 is the initial sample length (mm), and L_T is the sample length (mm) at temperature T. The ASR is calculated in accordance with eq 3

https://doi.org/10.1021/acsomega.2c06808
ACS Omega 2023, 8, 5545−5552

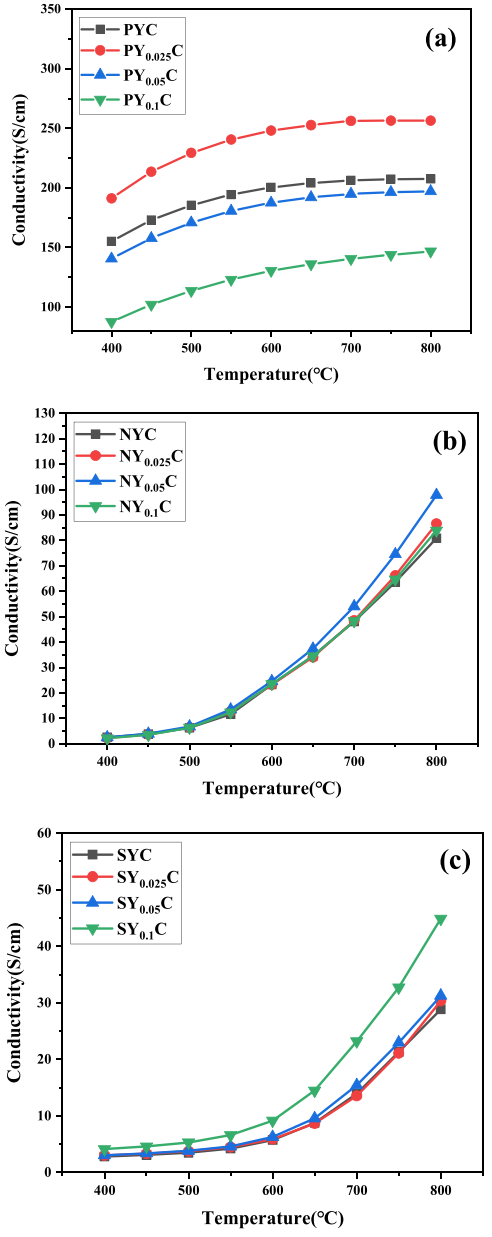

Figure 4. Variation curve of conductivity with the temperature of LY_xC (x = 0−0.1) series cathode materials: (a) PY_xC (x = 0−0.1); (b) NY_xC (x = 0−0.1); and (c) SY_xC (x = 0−0.1).

Table 1. Average CTE of LY_xC (x = 0−0.1) Series Cathode Materials

samples	average CTE ($\times 10^{-6}$ K^{-1})
PYC	13.382
$PY_{0.025}C$	13.248
$PY_{0.05}C$	12.812
$PY_{0.1}C$	12.489
NYC	14.549
$NY_{0.025}C$	14.523
$NY_{0.05}C$	14.493
$NY_{0.1}C$	14.029
SYC	14.450
$SY_{0.025}C$	14.228
$SY_{0.05}C$	14.118
$SY_{0.1}C$	13.830

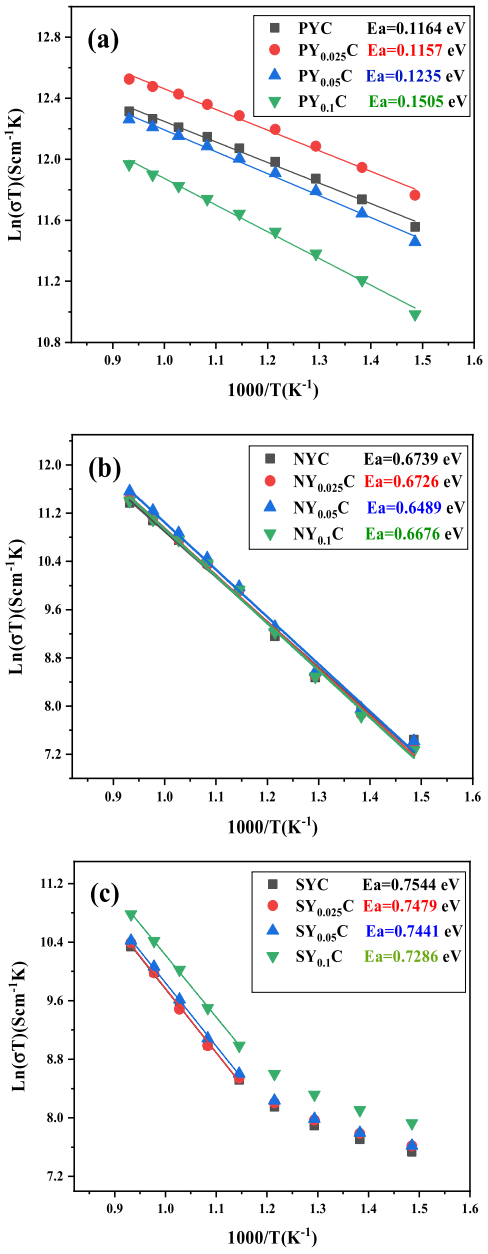

Figure 5. Arrhenius curves for the conductivity of LY_xC (x = 0−0.1): (a) PY_xC (x = 0−0.1); (b) NY_xC (x = 0−0.1); and (c) SY_xC (x = 0−0.1).

$$\mathrm{ASR} = \frac{R_p \times S}{2} \tag{3}$$

where R_p is the polarization impedance (Ω) measured in the impedance spectrum and S is the effective area (cm^2) of the cathode on one side of a symmetric cell.

3. RESULTS AND DISCUSSION

The X-ray diffraction (XRD) patterns of LY_xC (x = 0−0.1) series cathode materials are shown in Figure 1. The diffraction peaks of LY_xC (x = 0−0.1) cathode materials correspond to the standard diffraction card, and no other impurity peaks are generated, indicating that Y^{3+} has successfully replaced parts of Pr^{3+}, Nd^{3+}, and Sm^{3+}. From the local amplification patterns of XRD, the diffraction peaks of the cathode materials shift to a higher angle, indicating that the cell volume is reduced. This

https://doi.org/10.1021/acsomega.2c06808
ACS Omega 2023, 8, 5545−5552

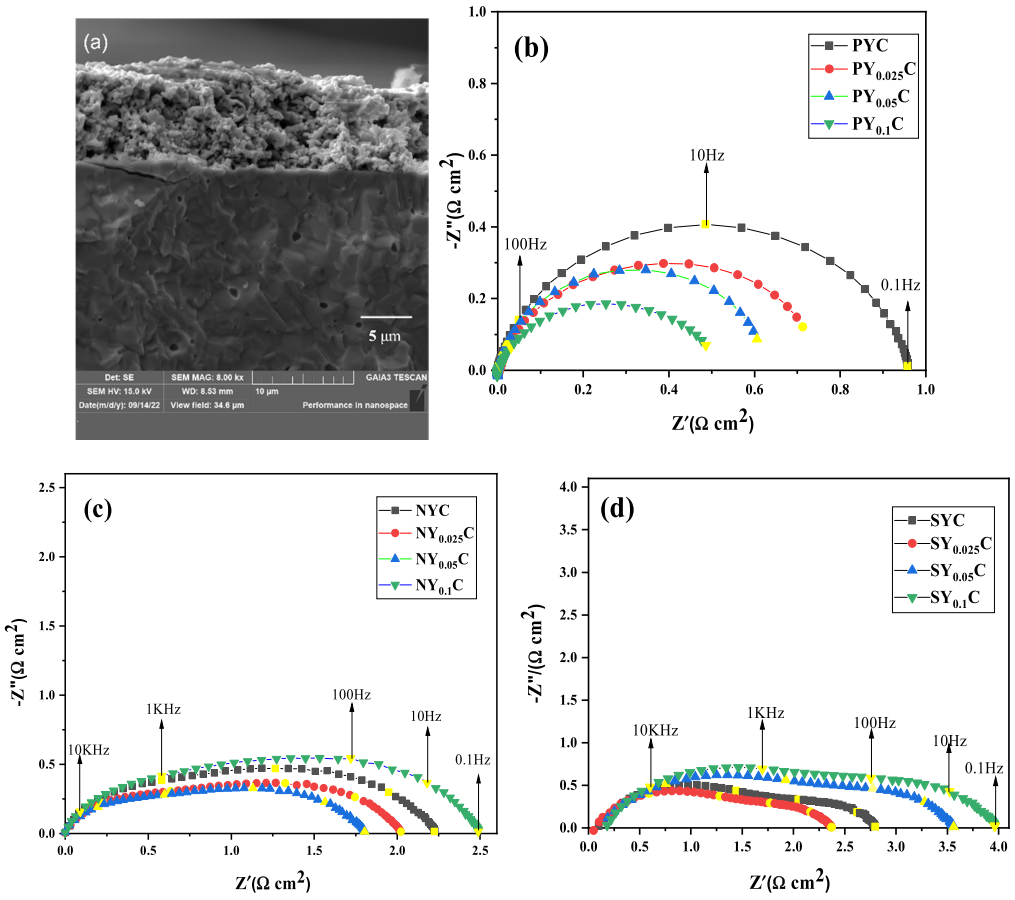

Figure 6. SEM and Ac impedance spectra of LY_xC (x = 0−0.1) cathode materials at 800 °C: (a) cross-sectional SEM images; (b) PY_xC (x = 0−0.1); (c) NY_xC (x = 0−0.1); (d) SY_xC (x = 0−0.1).

phenomenon can be attributed to the following conditions: the ion radii, Y^{3+}(IX) = 1.075 Å, Pr^{3+}(IX) = 1.179 Å, Nd^{3+}(IX) = 1.163 Å, and Sm^{3+}(IX) = 1.132 Å (Roman numerals represent the coordination number).[13] With the doping of Y^{3+} with a small ionic radius into Sm^{3+}, Pr^{3+}, and Nd^{3+} with large ionic radii at the A site, the A−O bond is shortened, the average radius of the A-site ion is reduced, and the cell volume is reduced. For the undoped cathode material, the cell volumes of the three elements Pr, Nd, and Sm decrease successively due to their ionic radii.

The compatibility of $PY_{0.025}C$, $NY_{0.025}C$, and $SY_{0.025}C$ cathodes with SDC was tested. As shown in Figure 2, the diffraction peaks of the mixed materials are all those of $PY_{0.025}C$, $NY_{0.025}C$, $SY_{0.025}C$, and SDC, which indicates that LY_xC (x = 0−0.1) series cathode materials do not react with SDC and have good chemical compatibility.

Figure 3 shows the thermal expansion curves of LY_xC (x = 0−0.1) series cathode materials. The average CTE is calculated at 200−800 °C, and the calculation results are shown in Table 1. As shown in Figure 3, the thermal expansion curves of LY_xC series cathode materials are all simple linear relations, indicating that phase transition does not occur with the increase in temperature. As shown in Table 1, the average CTE of LY_xC (x = 0−0.1) series cathode materials decreases gradually with the increase in the Y^{3+} doping amount. This phenomenon may be due to two reasons. First, Y^{3+} with a smaller ionic radius occupies the positions of Pr^{3+}, Nd^{3+}, and Sm^{3+} with larger radii, which causes the lattice shrinkage and reduces the CTE of the sample. Second, the higher the strength of the ionic bond in the lattice, the smaller the CTE value.[14] The Y−O bond has stronger ionic bond energy than Pr−O, Nd−O, and Sm−O bonds, so the increase in the Y^{3+} doping amount leads to the decrease in CTE.[15]

At the temperature range of 400−800 °C in air, the conductivity curve of LY_xC (x = 0−0.1) series cathode materials varies with temperature, as shown in Figure 4. In the process of temperature rise, the electrical conductivity of LY_xC (x = 0−0.1) series cathode materials increases with the increase in temperature, showing semiconductor conductive behavior. This phenomenon is because the increase in temperature accelerates the electrode reaction and increases the mobility of charge carriers (i.e., electron holes). As shown in Figure 4, the conductance of PY_xC (x = 0−0.1) and NY_xC (x = 0−0.1) cathodic materials first increases and then decreases, whereas the conductance of SY_xC (x = 0−0.1) cathodic materials increases continuously. The electron conduction path is along the BO_6 octahedral unit, and the distance between the B-site cations is strongly related to the electron−hole migration.[16] The phenomenon that the conductivity increases with the increase in Y^{3+} doping amount may be explained by the fact that Y^{3+} doping reduces the cell volume, shortens the spacing between adjacent BO_6 octahedra, and enables the electron−hole transition, thereby showing higher conductivity.[17] The decrease in conductivity may be due to the increase in the Y^{3+} doping amount, which decreases the spacing between adjacent BO_6 octahedra and leads to a denser nucleus. Although the carrier transition is easier, it increases the probability that the carrier is blocked by the nucleus during the migration, and the blocking

https://doi.org/10.1021/acsomega.2c06808
ACS Omega 2023, 8, 5545−5552

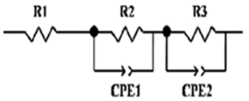

Figure 7. Equivalent circuit for the fitting impedance spectrum.

probability is more remarkable, resulting in a decrease in conductivity. From the comparison in Figure 4, the PY_xC (x = 0−0.1) cathode material has the highest conductivity, which exceeds 100 S·cm^{-1}, and is more suitable as a cathode material.

The Arrhenius curves of the conductivity of LY_xC series materials are shown in Figure 5. As can be seen from the figure, the conductivity of the material almost satisfies a linear relationship with temperature in the temperature range of 400−800 °C, which belongs to the small polarizer jump conduction mechanism. The conductivity activation energy of the LY_xC (L = Pr,Nd) cathode material decreases and then increases with the increase of Y^{3+} doping. The activation energy of SY_xC decreases with the increase of the doping amount in accordance with the trend of the measured conductivity.

Figure 6a shows the cross-sectional SEM image of the fabricated |SDC| cathode symmetric cells, revealing the interface between the cathode layer (LY_xC) and dense SDC electrolyte. It can be seen that the cathodes possess highly porous structures as designed. More importantly, the porous cathodes and the dense SDC electrolyte were well-coupled at their interfaces in all cells.[18] This ensures that the electrochemical testing results of these cells reveal the intrinsic properties of these cathodes. The AC impedance spectra of LY_xC (x = 0−0.1) series cathode materials at 800 °C are shown in Figure 6b−d to judge the polarization impedance changes in cathode materials with different doping ratios. With the increase in the Y^{3+} doping amount, the polarization impedance of the PY_xC (x = 0−0.1) cathode material gradually decreases, whereas the polarization impedance of the NY_xC (x = 0−0.1) and SY_xC (x = 0−0.1) cathode materials decreases first and then increases, indicating that doping Y^{3+} within a certain range can reduce the polarization impedance of cathode material, and the catalytic activity of the oxygen reduction of cathode materials is improved. The polarization phase transition of crystal grain and boundary response is extremely small, and the charge transfer is extremely fast due to the rapid polarization process, so the high frequency cannot be shown in the impedance diagram.[19] As shown in Figure 6, the impedance spectra of NY_xC (x = 0−0.1) and SY_xC (x = 0−0.1) have two obvious arcs of medium and low frequencies. PY_xC (x = 0−0.1) only exhibits one arc, which is the same as Sadykov,[20] and is only fitted in accordance with an intermediate-frequency reaction process.

Nova software is used to fit the equivalent circuit diagram of the AC impedance spectra, as shown in Figure 7. In the circuit, R1 is the ohmic impedance of electrolyte and wire, and CPE1 and CPE2 correspond to the intermediate-frequency and low-frequency constant phase components, respectively. R2 and R3 are polarization resistors with intermediate and low frequencies, respectively.[21] R2 represents the transport of oxygen ions through the cathode, and R3 represents the nonchemical processes, such as oxygen adsorption and dissociation. R_p is the polarization impedance, and R_p = R2 + R3.

The ohmic impedance of the electrolyte and the wire is normalized because only the polarization impedance related to the oxygen reduction reaction is considered.[22] Figure 8 shows the relationship between the polarization impedance and

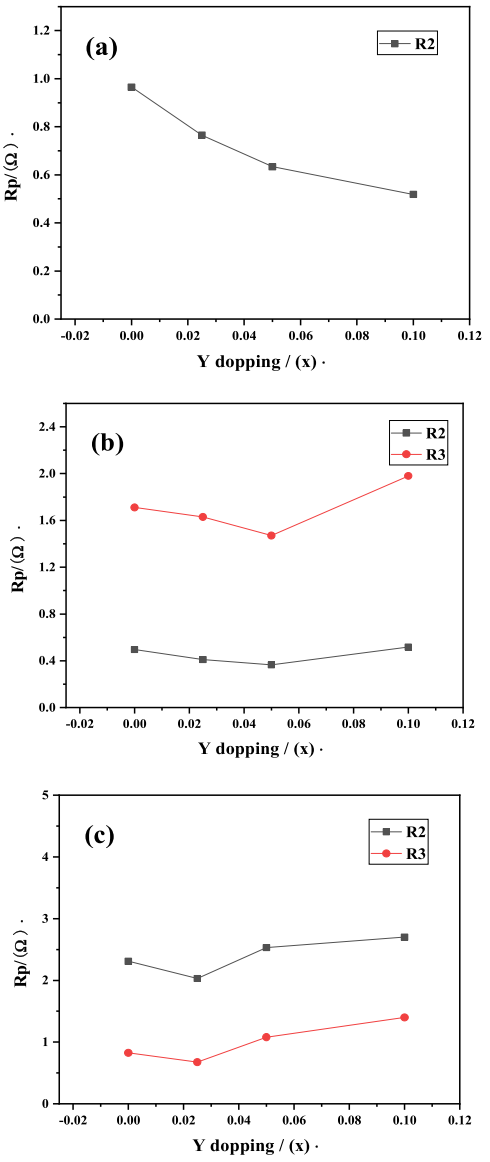

Figure 8. Relationship between Y^{3+} doping and polarization impedance of LY_xC (x = 0−0.1): (a) PY_xC (x = 0−0.1) cathode material; (b) R2 is less than R3 for the NY_xC (x = 0−0.1) cathode; and (c) R2 is larger than R3 for the SY_xC (x = 0−0.1) cathode.

temperature of LY_xC (x = 0−0.1) cathode material after fitting. As shown in Figure 8a, the PY_xC (x = 0−0.1) cathode material mainly carries out oxygen ion transport inside the cathode at 800 °C. As shown in Figure 8b, R2 is less than R3 for the NY_xC (x = 0−0.1) cathode material, which indicates that the transport capacity of oxygen ions in the cathode is stronger than the adsorption and dissociation capacity of oxygen at 800 °C. As shown in Figure 8c, R2 is larger than R3 for the SY_xC (x = 0−0.1) cathode material, indicating that the oxygen adsorption and dissociation of this material are dominant at 800 °C. The polarization impedance decreases probably due to the increase in the doping amount of Y^{3+}, which decreases the oxygen content and causes the loss of the part of lattice oxygen and increases the oxygen vacancies, thereby improving the transport performance of oxygen ions.[23] The increase in polarization impedance may be due to Y^{3+} doping with a small radius and the shortening of the A−O bond, which reduces the distance between the intergap site oxygen ions and the vertices of BO_6

https://doi.org/10.1021/acsomega.2c06808
ACS Omega 2023, 8, 5545−5552

Table 2. ASR ($\Omega.cm^2$) of LY_xC (x = 0−0.1) Series Cathode Materials at 800 °C

samples	x = 0	x = 0.025	x = 0.05	x = 0.1
PY_xC	0.379	0.301	0.249	0.204
NY_xC	0.865	0.801	0.720	0.981
SY_xC	1.229	1.168	1.417	1.609

regular octahedron, thereby reducing the oxygen ion transport capacity.[24] Table 2 shows the ASR value of LY_xC series cathode materials at 800 °C. PY_xC (x = 0−0.1) has the smallest ASR value, whereas SY_xC (x = 0−0.1) has the largest ASR value because the radius reduction of Ln^{3+} (Pr, Nd, Sm) results in the reduction of oxygen vacancy content and the increase in polarization impedance.[25]

4. CONCLUSIONS

The A site of the $Ln_2CuO_{4+\delta}$ cathode material was doped with Y^{3+} and the electrochemical performance was investigated. The average CTE decreases gradually with the gradual decrease in the cell volume of Y^{3+}-doped $Ln_{2-x}Y_xCuO_{4+\delta}$ (Ln = Pr, Nd, Sm; x = 0, 0.025, 0.05, 0.1) cathode material. Y^{3+} doping can effectively improve the conductivity of the cathode material. $Pr_{1.975}Y_{0.025}CuO_{4+\delta}$ has the highest conductivity at 800 °C (256 $S{\cdot}cm^{-1}$), which is about 25% higher than the conductivity of the undoped cathode (204 $S{\cdot}cm^{-1}$). The doping of Y^{3+} improves the oxygen reduction catalytic activity of the cathode material. The ASR value of $Pr_{1.9}Y_{0.1}CuO_{4+\delta}$ at 800 °C is the lowest, which is 0.204 $\Omega{\cdot}cm^2$. Compared with Nd and Sm, Pr as an A-site doping material has better thermal stability and electrochemical performance, which is more suitable for SOFC cathode materials.

AUTHOR INFORMATION

Corresponding Author

Songbo Li − *Inner Mongolia University of Science and Technology, Baotou 014010, China*; orcid.org/0000-0001-7603-3042; Email: songboli2021@hotmail.com

Authors

Yang Ni − *Inner Mongolia University of Science and Technology, Baotou 014010, China*

Shengli An − *Inner Mongolia University of Science and Technology, Baotou 014010, China*

Xu Du − *Inner Mongolia University of Science and Technology, Baotou 014010, China*

Liangmei Xue − *Inner Mongolia University of Science and Technology, Baotou 014010, China*

Complete contact information is available at: https://pubs.acs.org/10.1021/acsomega.2c06808

Notes

The authors declare no competing financial interest.

ACKNOWLEDGMENTS

The work was supported by the National Natural Science Foundation of China (No: 51974167) and the Scientific Research Program of Inner Mongolia Higher Education Institutions (NJZZ22449).

REFERENCES

(1) Ding, X. F.; Li, M. N.; Zhao, X. Y.; Ding, L. M.; Yan, Y. F.; Wang, L. X.; Wang, Z. H. A highly active and stable cathode for oxygen reduction in intermediate temperature solid oxide fuel cells. *Sustainable Energy Fuels* **2020**, *4*, 1168−1179.

(2) Santos-Gómez, L. D.; Porras-Vázquez, J. M.; Hurtado, J.; Losilla, E. R.; Marrero-López, D. Stability and electrochemical performance of nanostructured $La_2CuO_{4+\delta}$ cathodes. *J. Alloys Compd.* **2019**, *788*, 565−572.

(3) Torres-Garibay, C.; Kovar, D.; Manthiram, A. $Ln_{0.6}Sr_{0.4}Co_{1-y}Fe_yO_{3-\delta}$ (Ln = La and Nd;y = 0 and 0.5) cathodes with thin yttria-stabilized zirconia electrolytes for intermediate temperature solid oxide fuel cells. *J. Power Sources* **2009**, *187*, 480−486.

(4) Kim, J. H.; Manthiram, A. $LnBaCo_2O_{5+\delta}$ oxides as cathodes for intermediate-temperature solid oxide fuel cells. *J. Electrochem. Soc.* **2008**, *155*, No. B385.

(5) Hu, X. Y.; Li, M.; Xie, Y.; Yang, Y.; Wu, X. J.; Xia, C. R. Oxygen deficient ruddlesden-popper-type lanthanum strontium cuprate doped with bismuth as a cathode for solid oxide fuel cells. *ACS Appl. Mater. Interfaces* **2019**, *11*, 21593−21602.

(6) Kamecki, B.; Karczewski, J.; Jasiński, P.; Molin, S. Improvement of oxygen electrode performance of intermediate temperature solid oxide cells by spray pyrolysis deposited active layers. *Adv. Mater. Interfaces* **2021**, *8*, No. 2002227.

(7) Boehm, E.; Bassat, J. M.; Dordor, P.; Mauvy, F.; Grenier, J. C.; Stevens, P. Oxygen diffusion and transport properties in non-stoichiometric $Ln_{2-x}NiO_{4+\delta}$ oxides. *Solid State Ionics* **2005**, *176*, 2717−2725.

(8) Skinner, S. J.; Kilner, J. A. Oxygen diffusion and surface exchange in $La_{2-x}Sr_xNiO_{4+\delta}$. *Solid State Ionics* **2000**, *135*, 709−712.

(9) Yang, G. M.; Su, C.; Shi, H. G.; Zhu, Y. L.; Song, Y. F.; Zhou, W.; Shao, Z. P. Toward reducing the operation temperature of solid oxide fuel cells: our past 15 years of efforts in cathode development. *Energy Fuels* **2020**, *34*, 15169−15194.

(10) Fu, Y. P.; Subardi, A.; Hsieh, M. Y.; Chang, W. K. Electrochemical properties of $La_{0.5}Sr_{0.5}Co_{0.8}M_{0.2}O_{3-\delta}$ (M = Mn, Fe, Ni, Cu) perovskite cathodes for IT-SOFCs. *J. Am. Ceram. Soc* **2016**, *99*, 1345−1352.

(11) Gao, L.; Zhu, M.; Li, Q.; Sun, L.; Zhao, H.; Grenier, J. C. Electrode properties of Cu- doped $Bi_{0.5}Sr_{0.5}FeO_{3-\delta}$ cobalt-free perovskite as cathode for intermediate-temperature solid oxide fuel cells. *J. Alloys Compd.* **2017**, *700*, 29−36.

(12) Yuan, M. H.; Dong, W. J.; Wei, L. L.; Liu, Q.; Meng, Y. J.; Wang, X. Y.; Wang, B. Y.; Zhu, B. Stability study of SOFC using layered perovskite oxide $La_{1.85}Sr_{0.15}CuO_4$ mixed with ionic conductor as membrane. *Electrochim. Acta* **2020**, *332*, No. 135487.

(13) Zhang, X. N.; Xia, T.; Li, Q.; Sun, L. P.; Huo, L. H.; Zhao, H. A highly active and CO_2-tolerant perovskite cathode for solid oxide fuel cells operating below 700 °C. *J. Alloys Compd.* **2021**, *858*, No. 157743.

(14) Zhao, H. L.; Zheng, Y.; Yang, C. Y.; Shen, Y. N.; Du, Z. H.; Swierczek, K. Electrochemical performance of $Pr_{1-x}Y_xBaCo_2O_{5+\delta}$ layered perovskites as cathode materials for intermediate-temperature solid oxide fuel cells. *Int. J. Hydrogen Energy* **2013**, *38*, 16365−16372.

(15) Benamira, M.; Ringuedé, A.; Cassir, M.; Horwat, D.; Lenormand, P.; Ansart, F.; Bassat, J. M.; Viricelle, J. P. Enhancing oxygen reduction reaction of YSZ/$La_2NiO_{4+\delta}$ using an ultrathin $La_2NiO_{4+\delta}$ in terfacial layer. *J. Alloys Compd.* **2018**, *746*, 413−420.

(16) Duan, Z.; Zhu, Y.; Hu, Z.; Zhang, J.; Liu, D.; Luo, X.; Gao, M.; Lei, L.; Wang, X.; Zhao, G. Micro-patterned $NiFe_2O_4$/Fe−TiO_2 composite films: Fabrication, hydrophilicity and application in visible-light-driven photocatalysis. *Ceram. Int.* **2020**, *46*, 27080−27091.

(17) Wang, Z. W.; Sun, H. B.; Li, J.; Guo, H.; Li, G. C. Modified $La_{0.6}Sr_{0.4}Co_{0.2}Fe_{0.8}O_{3-\delta}$ cathodes with the infiltration of $Er_{0.4}Bi_{1.6}O_3$ for intermedi-ate-temperature solid oxide fuel cells. *Int. J. Hydrogen Energy* **2021**, *46*, 22932−22941.

(18) Ortiz-Vitoriano, N.; de Larramendi, I. R.; Cook, S. N.; Burriel, M.; Aguadero, A.; Kilner, J. A.; Rojo, T. The formation of performance enhancing pseudo-composites in the highly active $La_{1-x}Ca_xFe_{0.8}Ni_{0.2}O_3$ system for IT-SOFC application. *Adv. Funct. Mater* **2013**, *23*, 5131−5139.

(19) Lenka, R. K.; Patro, P. K.; Patel, V.; Muhmood, L.; Mahata, T. Comparative investigation on the functional properties of alkaline earth

metal (Ca, Ba, Sr) doped $Nd_2NiO_{4+\delta}$ oxygen electrode material for SOFC applications. *J. Alloys Compd.* **2021**, *860*, No. 158490.
(20) Sadykov, V. A.; Pikalova, E. Y.; Kolchugin, A. A.; Fetisov, A. V.; Sadovskava, E. M.; Filonova, E. A.; Eremeev, N. F.; Goncharov, V. B.; Krasnov, A. V.; Skriabin, P. I.; et al. Transport properties of Ca-doped Ln_2NiO_4 for intermediate temperature solid oxide fuel cells cathodes and catalytic membranes for hydrogen production. *Int. J. Hydrogen Energy* **2020**, *45*, 13625−13642.
(21) Pers, P.; Mao, V.; Taillades, M.; Taillades, G. Electrochemical behavior and performances of Ni-$BaZr_{0.1}Ce_{0.7}Y_{0.1}Yb_{0.1}O_{3-\delta}$ cermet anodes for protonic ceramic fuel cell. *Int. J. Hydrogen Energy* **2018**, *43*, 2402−2409.
(22) Kim, S. J.; Kim, K. J.; Choi, G. M. A novel solid oxide electrolysis cell (SOEC) to separate anodic from cathodic polarization under high electrolysis current. *Int. J. Hydrogen Energy* **2015**, *40*, 9032−9038.
(23) Sun, C. Z.; Kong, Y.; Shao, L.; Sun, K. N.; Zhang, N. Q. Probing oxygen vacancy effect on oxygen reduction reaction of the $NdBaCo_2O_{5+\delta}$ cathode for solid oxide fuel cells. *J. Power Sources* **2020**, *459*, No. 228017.
(24) Zhang, W.; Zhou, Y.; Hussain, A. M.; Song, D.; Liu, M.; Chen, Y.; Luo, Z.; Kane, N.; Niu, Y.; Dale, N.; Fukuyama, Y.; Liu, M. High-performance, thermal cycling stable, coking-tolerant solid oxide fuel cells with nanostructured electrodes. *ACS Appl. Mater. Interfaces* **2021**, *13*, 4993−4999.
(25) Wang, S. L.; Zan, J. N.; Qiu, W. W.; Zheng, D. S.; Li, F. S.; Chen, W. M.; Pei, Q. M. Evaluation of perovskite oxides $LnBaCo_2O_{5+\delta}$ (Ln = La, Pr, Nd and Sm) as cathode materials for IT-SOFC. *J. Electroanal. Chem* **2021**, *886*, No. 115144.

https://doi.org/10.1021/acsomega.2c06808
ACS Omega 2023, 8, 5545−5552